Optical anisotropy of semiconductor nanowires beyond the electrostatic limit

J. Zhang, A. A. Lutich, J. Rodríguez-Fernández, A. S. Susha,* A. L. Rogach,* F. Jäckel,† and J. Feldmann
Photonics and Optoelectronics Group, Department of Physics and CeNS, Ludwig-Maximilians-Universität München, Amalienstr. 54, 80799 Munich, Germany

(Received 6 May 2010; revised manuscript received 25 August 2010; published 1 October 2010)

Semiconductor nanowires with diameters below 100 nm exhibit distinct polarization anisotropies that cannot be explained in the electrostatic limit. Comparing experiments with calculations reveals the effects of diameter-wavelength ratio, material dispersion, and local refractive index. All these parameters need to be taken into account to fully understand optical anisotropies in the size regime between extremely thin nanowires and bulklike materials.

DOI: 10.1103/PhysRevB.82.155301 PACS number(s): 81.07.Gf, 78.55.−m, 78.35.+c

I. INTRODUCTION

Semiconductor nanowires (NWs) have received increasing attention in the last decade since their quasi-one-dimensional shape is attractive for electronic transport, sensing, and polarization sensitive applications, as well as fundamental studies.[1–3] NWs with various chemical composition, a range of diameters, and aspect ratios have been prepared through liquid vapor deposition, laser assisted catalytic growth, synthesis in solution as well as self-assembly techniques.[4–6] Of particular interest are the optical properties of NWs that are determined to a large extent by their high aspect ratio. Large polarization anisotropies of excitation, photoluminescence (PL), and photoconductivity have been reported.[7,8] This renders NWs promising materials for polarization sensitive optical and optoelectronic applications. At NW diameters smaller than the exciton Bohr radius confinement-induced mixing of valence band states contributes to the optical anisotropy.[9,10] At larger diameters, still much smaller than the wavelength of light in the material, a purely electrostatic model usually explains the polarization anisotropy.[7] The latter model is based on the anisotropic dielectric mismatch of the nanowire with its environment, i.e., an anisotropic refractive index "contrast," which leads to different optical confinement of light with different polarization. Only recently, the polarization properties of NWs with diameters comparable to the wavelength of light in the NW material started to attract interest since size-dependent effects, absent both for very thin NWs and bulklike material, can be expected.[11–16] A number of studies focused on NWs with diameters large enough to support resonant, i.e., wave guiding, modes within the NWs for a given wavelength. For such NWs an oscillatory behavior of the polarization anisotropy is predicted,[11] and anisotropy and enhancement of Raman scattering,[16] and whispering gallery modes[15] have been reported. However, the electrostatic limit is expected to break down already at much smaller NW diameters at which resonant guided modes are not significant. In this size regime only recently first investigations into the role of leaky modes,[14] as well as size dependencies appeared.[12,13] Due to the large refractive index of most semiconductor materials in the UV-Vis spectral range ($n>3$) these effects are expected already at NW diameters below 100 nm.

Here, we report on the polarization anisotropies in excitation, photoluminescence, and Rayleigh scattering from polycrystalline CdTe NWs prepared from colloidal semiconductor nanocrystals (SNCs) via self-assembly in solution. We study the optical anisotropy for individual NWs as well as for ensembles of NWs aligned in polymer films. We find that the observed anisotropies cannot be explained in the electrostatic limit, i.e., when neglecting the NW diameter. We perform finite-difference time domain (FDTD) calculations with realistic parameters for the CdTe NWs for excitation and photoluminescence anisotropy in order to explain the observed anisotropies. The comparison between theory and experiment reveals that the NW diameter-wavelength ratio, the material dispersion of the NW (i.e., the wavelength dependency of the refractive index) as well as the local refractive index of the surrounding need all to be taken into account to fully understand the anisotropies observed.

II. EXPERIMENTAL

CdTe SNCs were prepared according to published procedures and used to prepare polycrystalline NWs via partial destabilization of the organic ligand shell (thioglycolic acid) with physiological phosphate-buffered saline solution (PBS buffer).[17,18] The partially destabilized SNCs self-assemble in solution to form polycrystalline NWs in which both SNCs and remaining ligands are present to form a composite material. NWs were dispersed at ultralow concentrations on silicon or glass substrates for single NW measurements. Aligned ensembles of NWs were prepared similar to reported procedures.[19] In short, NWs were added to a 7.5 wt % polyvinylalcohol (PVA) aqueous solution. The mixture was dropped on a glass substrate and allowed to dry within 24 h. The resulting film was removed from the substrate, heated to 30 °C and then stretched in one direction until its length increased by ~50%. Typical lateral dimensions of the stretched film were between 1 and 2 cm with thicknesses around 50 μm.

Excitation and PL measurements of individual NWs were performed on a homebuilt wide-field fluorescence microscope using the frequency doubled output of a Ti-Sapph laser (Tsunami, Spectra Physics) at 415 nm for excitation, as depicted in Fig. 1(a). Rayleigh scattering of all samples and excitation and PL measurements of aligned NW ensembles were performed on a combined dark-field/laser microscope as shown in Fig. 1(b). PL of NW arrays was excited with the

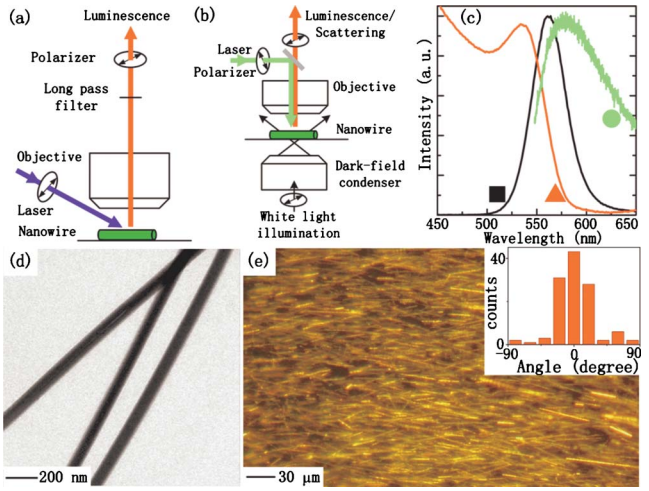

FIG. 1. (Color online) [(a) and (b)] Sketches of the wide-field luminescence and combined dark-field/laser microscope, respectively. (c) Absorption (red, triangle) and PL (black, square) spectra of the SNCs in solution (starting material to prepare the NWs) and typical PL spectrum of a single NW (green, circle). (d) TEM image of NWs and (e) Rayleigh scattering image of NWs aligned in a PVA film, inset: distribution of the angle between the long axis of individual NWs and the alignment direction in the PVA film.

second harmonic of a diode-pumped Nd:YAG laser at 532 nm. In both setups, polarizers were placed in either the excitation or detection path, respectively. Isotropically absorbing, emitting, and scattering test samples were used to correct for the intrinsic polarization effects of the optics in each setup. FDTD calculations were performed using the free software package MEEP.[20,21]

III. RESULTS

Figs. 1(a) and 1(b) illustrate the experimental setups of the wide-field luminescence and combined dark-field/laser microscope, respectively. Figure 1(c) displays the absorption and PL spectra of the CdTe SNCs (3.1 nm in diameter) that were used to prepare polycrystalline NWs as well as a typical PL spectrum of an individual NW. The PL of NWs is redshifted and broadened compared to the PL of the SNCs in solution. The redshift is due to electronic coupling between the SNCs constituting the polycrystalline NWs while the broadening has been attributed to the disorder in the polycrystalline NWs.[22] The electronic coupling between the SNCs is dominated by exchange, i.e., tunneling, interaction as recently demonstrated by combined temperature dependent PL measurements and semiempirical calculations.[22] A representative TEM image of the obtained NWs is shown in Fig. 1(d). The NWs are several micrometers long and have an average diameter of 90 nm with a standard deviation of 20 nm as determined from the TEM images. This diameter range is on the same order of magnitude as the wavelength of visible light in, the high refractive index, CdTe. The NWs are polycrystalline[22] (no high-resolution TEM images shown here) since the organic ligands in the starting material are not completely removed.[17] The NWs thus consist of individual

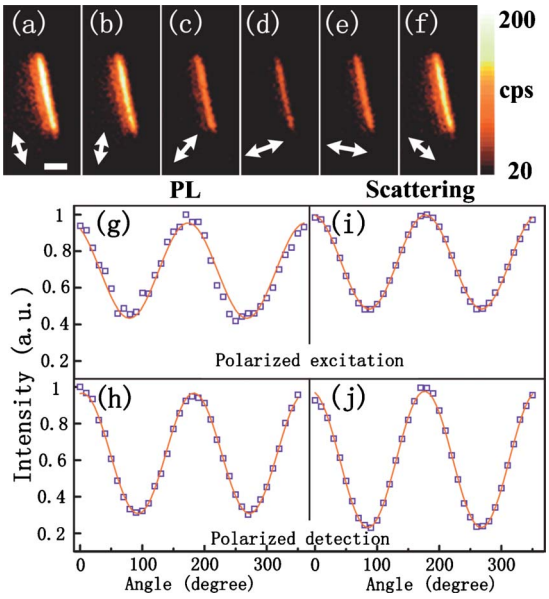

FIG. 2. (Color online) [(a)–(f)] Wide-field PL images of an individual NW for different excitation polarizations as indicated by the arrow (raw data). The scale bar is 5 μm. [(g) and (h)] PL intensity under linearly polarized excitation or detection, respectively, of the same individual NW shown in (a)–(f). The angle is measured with respect to the long axis of the NW. [(i) and (j)] Rayleigh-scattering intensity of an individual NW under polarized excitation and detection, respectively. Squares are experimental data, and curves are best fits to $\sin^2$ functions.

SNCs with different relative orientations of their crystal lattices,[22] and interstitial organic material filling the spaces in between.[17] Figure 1(e) displays a Rayleigh scattering image of NWs aligned in a PVA film. The NWs can be clearly recognized as bright elongated objects of high scattering intensity. The inset is a histogram of the angle between NWs in representative areas of the film with respect to the alignment direction. The standard deviation of this distribution is $\sim 30°$.

Figure 2 illustrates the polarization anisotropy data obtained from individual NWs. Figures 2(a)–2(f) show PL images of an individual NW under varying orientations of the linearly polarized laser excitation as indicated by the arrow in each panel. It can be clearly seen that the PL is largest for polarization along the long axis of the NW and smallest for perpendicular excitation. Figure 2(g) quantifies the PL intensity for a larger number of excitation angles. The angular dependence, like all the following dependencies, can be well fitted by $\sin^2$-functions. The polarization anisotropy

$$P = \frac{I_{\max} - I_{\min}}{I_{\max} + I_{\min}} \tag{1}$$

in excitation for this NW as calculated from the fit parameters is 0.37.[23] Upon excitation of the same NW with circularly polarized light and a polarizer in the detection path the curve displayed in Fig. 2(h) is obtained. The polarization anisotropy for the emission (P=0.52) is larger than for the excitation. This observation is the same for all the individual NWs investigated which show on average a polarization an-

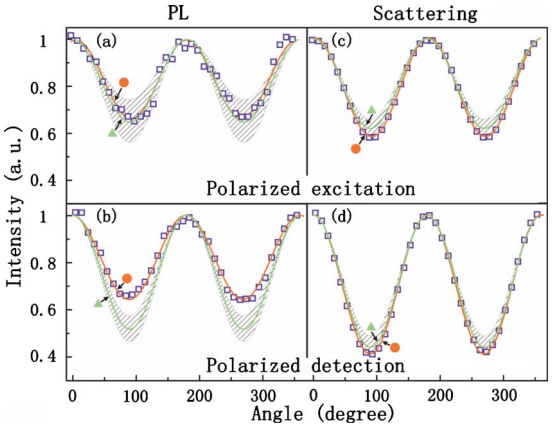

FIG. 3. (Color online) PL intensity of NW ensembles aligned in polymer films under: (a) under linearly polarized excitation and (b) linearly polarized detection. [(c) and (d)] Rayleigh scattering of these films with a polarizer in the excitation and detection paths, respectively. Blue squares are experimental data, red curves marked with circles are best fits to $\sin^2$ functions, and green curves marked with triangles are the expected polarization anisotropies based on average single NW polarization anisotropy convoluted with the orientational distribution from the inset in Fig. 1(e). The shaded areas represent expected standard deviation based on average single NW data.

isotropy of 0.48 ± 0.07 and 0.32 ± 0.10 for emission and excitation, respectively. Furthermore, the Rayleigh scattering of individual NWs is also polarized as evidenced by Figs. 2(i) and 2(j) for measurements on a single NW with a polarizer in the excitation and detection path, respectively. The polarization anisotropies of the NW in Figs. 2(i) and 2(j) are 0.34 and 0.61. The corresponding average values for all NWs are 0.58 ± 0.06 and 0.35 ± 0.04. Again, for all wires the anisotropy is larger for the polarized detection.

The same set of measurements has also been performed for NW ensembles aligned in PVA films of which the results are summarized in Fig. 3. As expected from the single NW experiments the films also show pronounced polarization anisotropies in excitation, emission, and Rayleigh scattering and the same trends, i.e., larger anisotropy if the polarizer is in the detection path, are observed. The anisotropies themselves (0.20 for PL excitation, 0.22 for PL emission, 0.26 for scattering excitation and 0.42 for scattering emission) are lower than for the single NWs.

IV. DISCUSSION

We first discuss the polarization anisotropies for individual NWs. In a simple electrostatic model the NW could be considered as uniform, infinite dielectric cylinder with dielectric constant ε and diameter d much smaller than the wavelength λ. Then the incident electric field E_0 would not be attenuated if polarized along the long axis of the NW. But if polarized perpendicular to the NW the attenuation would be given by[24]

$$E = \frac{2\varepsilon_0}{\varepsilon + \varepsilon_0} E_0. \tag{2}$$

With the dielectric constant of bulk CdTe between 12 and 9 in the UV-Vis spectral range, and neglecting substrate contributions, one would expect polarization anisotropies larger than 0.9.[25] This strongly suggests that the smaller polarization anisotropies reported above reflect the breakdown of the electrostatic approximation and that for a proper explanation the finite NW diameter needs to be taken into account.

We performed a series of FDTD calculations to include a finite NW diameter and explain our observations. The NW was modeled as a cylinder of dielectric constant ε_{eff} and diameter d and placed on a silica substrate ($\varepsilon_{silica}=2.13$). The polycrystalline nature of the NW was taken into account by estimating its effective dielectric constant using the Maxwell-Garnett approximation.[26] Here, we assumed that the SNCs in the NW are closely packed and occupy 74% of its volume.[22] With bulk dielectric constants for different wavelengths from the literature we find $\varepsilon_{eff}(400\ \text{nm})=8.3$ and $\varepsilon_{eff}(600\ \text{nm})=6.42$.[25] It should be noted that these effective dielectric constants still predict polarization anisotropies larger than 0.85 in the electrostatic approximation and thus significantly larger values than reported above. The simulated geometries are illustrated in the insets of Figs. 4(a) and 4(b). The polarization anisotropy in *excitation* was determined by comparing the average power density in the NW for an incident plane wave polarized either parallel or perpendicular to the long NW axis, respectively. Here, calculations were performed at 400 nm, close to the experimental excitation wavelength. The polarization anisotropy in *emission* was obtained from comparing the energy flux through the plane of a virtual detector originating from a point source placed inside the NW with its dipole moment parallel to the substrate and either parallel or perpendicular to the NW axis,

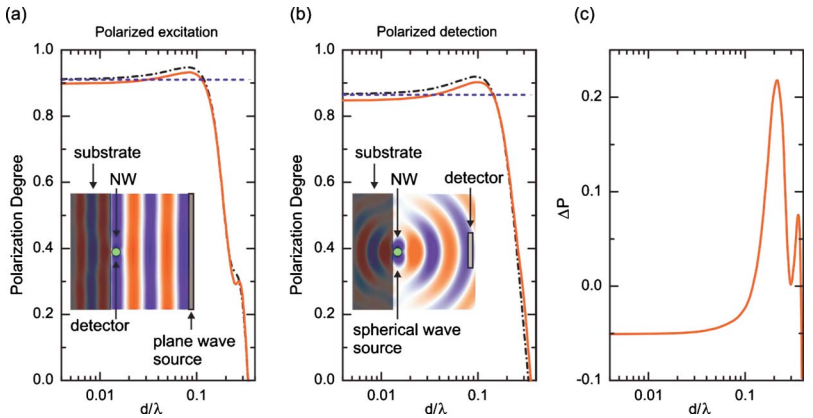

FIG. 4. (Color online) Calculated polarization anisotropy in (a) excitation and (b) emission as function of the NW diameter-to-vacuum wavelength ratio. Blue dashed curves represent the electrostatic limit without a substrate, red solid curves show FDTD calculations including the substrate, and black dashed-dotted curves are FDTD calculations without the substrate. (c) Difference of the polarization anisotropies in emission and excitation, i.e., difference between the solid curves in (a) and (b). Insets display the simulated geometries and snapshots of the field amplitude in the steady state.

respectively. Here, the calculations used a wavelength of 600 nm close to the PL maximum of the NWs. In the latter approach we do not include the anisotropy in excitation because we found that ensembles of SNCs immobilized on a substrate did *not* exhibit a polarized emission under linearly polarized excitation.

The results of the calculations are summarized in Fig. 4. Figure 4(a) displays the calculated polarization anisotropies in excitation as function of NW diameter-to-vacuum wavelength ratio d/λ. First, we point out that at the smallest ratios, i.e., thinnest NWs, our calculations without substrate perfectly reproduce the electrostatic limit and predict a polarization anisotropy of 0.9. The presence of the substrate lowers this anisotropy slightly since the refractive index contrast near the NW is reduced. At d/λ ratios larger than 0.05 significant differences are observed. First, the anisotropy slightly increases, and then, at ratios exceeding 0.1 sharply decreases, displaying a strong diameter dependence. For NWs with a diameter of 90 nm and an excitation wavelength of 400 nm our calculations predict a polarization anisotropy of $\sim$0.38 which is in excellent agreement with the observation of 0.32 ± 0.1 for individual NWs reported above. We therefore attribute the observed polarization anisotropies to the finite diameter of the NWs and the breakdown of the electrostatic limit associated with it. It should be noted that for NWs with even larger diameter large polarization anisotropies have been reported.[27,28] However, in these cases the origin of the anisotropies is either defect emission or guiding of waves within the NW. The latter situation, leading to oscillatory behavior of the anisotropies at large diameters, requires a minimum diameter for the support of guided modes in the studied spectral range.[11,29] For our NWs this limiting diameter is larger than the studied diameter range.

Figure 4(b) displays the calculation results for the polarization anisotropy in the emission. Qualitatively, the same behavior, i.e., agreement with the electrostatic limit at small d/λ ratios and sharp decrease in P at large d/λ ratios, is observed. Subtle but important differences can be found: first, both the electrostatic limit and our calculation now predict slightly lower polarization anisotropies for the thinnest NWs. This is due to the larger dielectric constant at shorter wavelength used in the excitation calculations. Second, the onset of the breakdown of the electrostatic limit occurs at larger d/λ ratios. This can be attributed to a larger "optical diameter" and a smaller optical contrast of the NW due to the longer wavelength used and the fact that the dielectric constant drops from 8.3 at 400 nm to 6.42 at 600 nm. Thus, the calculations predict a larger polarization anisotropy for the diameter regime of our NWs in emission than in excitation due to both a d/λ dependence of the polarization anisotropy and the material dispersion. This explains our observation that individual NWs show (on average) 50% higher anisotropies in the emission. The predicted difference of the polarization anisotropy in emission and excitation is further illustrated in Fig. 4(c) in which we show $\Delta P = P_{em} - P_{exc}$ as function of the d/λ ratio. Two facts should be noted: First, one sees again that at small d/λ ratios ratios P_{exc} is larger while for larger ones P_{em} is larger. Second, the largest diameter dependent differences are observed in the diameter range spanned by our NWs.

The polarization anisotropies in Rayleigh scattering are more complicated and we limit ourselves to a qualitative discussion here. The above calculations for the polarization anisotropy in excitation principally also apply here. One can expect an anisotropic excitation of classical scattering dipoles. These classical scattering dipoles will, similarly to the above calculations, lead to anisotropic scattering. However, the above material dispersion and wavelength based arguments are not valid anymore since polarized excitation and detection occur here over the same, much broader spectral range. In addition, with a polarizer in front of the dark field condenser the excitation polarization at the sample is not purely linearly polarized. Instead, there is only a dominant polarization component in the projection of the excitation light into the sample plane. Therefore, the observed lower polarization anisotropy in excitation is likely to contain a major component from this difference in excitation geometry.

Alternatively, one might explain the observed polarization anisotropies by anisotropic localization of excitons due to anisotropic disorder in the NWs. Indeed, excitons are expected to localize in the NWs at locally energetically favorable sites from where emission occurs.[30] The continuous PL emission intensity indicates that such sites exist along the whole wire. However, high-resolution TEM images (see Ref. 22) reveal no preferred orientation of the individual SNCs in the NWs in terms of their crystallographic axis. In addition, spherical SNCs generally do not exhibit linearly polarized emission.[31] In the present case, ensembles of isolated SNCs did not show polarized emission under linearly polarized excitation. We therefore discard the possibility that anisotropic localization and disorder plays a significant role in the polarization anisotropies reported and discussed here.

We now turn to the discussion of the polarization anisotropies of aligned ensembles of NWs. In general, the NW ensembles show lower polarization anisotropies than the corresponding single-NW measurements. This can be explained by considering the disorder in the aligned films, the presence of a higher refractive index matrix, i.e., the PVA, and multiple-scattering events. Figures 3(a)–3(d) display, next to the experimental data (squares) and best fits (red curves marked with circles), green curves marked with triangles. These curves were obtained from numerically convoluting the trace expected from an *average* individual NW with the angular distribution of the inset in Fig. 1(e) fitted to a Gaussian distribution. The shaded areas represent the standard deviation of the polarization anisotropies observed for individual NWs. For the polarization anisotropy in excitation and in Rayleigh scattering for both detection geometries we find agreement between the curves calculated from the single-NW data and the experimental data of the ensembles within one standard deviation. The polarization anisotropy in emission is slightly smaller for the ensembles than expected from the convoluted single-NW data. This good agreement, only considering the disorder in the films is surprising, since the presence of the PVA matrix is neglected. The matrix is expected to reduce the "refractive index contrast" with the NWs due to its refractive index being larger than 1. This should lead to a further decrease in the polarization anisotropy. We therefore tested the significance of the matrix ef-

fect by Rayleigh scattering from single NWs with a polarizer in the detection path. For the same individual NWs we obtained polarization anisotropies in air and in oil with a large refractive index of 1.518, respectively. Indeed, we found that for each NW the polarization anisotropy was significantly reduced in the higher refractive index medium. On average a reduction in 50% was observed. This confirms the matrix effect and suggests that in the films additional effects *increasing* the polarization anisotropy must be present. Since the films are tens of micrometers thick it can be expected that light passing through the film undergoes multiple-scattering events, each increasing the polarization anisotropy of the detected light. An alternative explanation for increased polarization anisotropy via the birefringence of stretched PVA films is considered unlikely since the differences in refractive index for the different polarization are small, typically on the order of 10^{-2} refractive index units.[32] We therefore attribute the polarization anisotropies in the polymer films to a combined effect of disorder, higher refractive index matrix, and multiple scattering.

V. CONCLUSION

In conclusion, we studied the polarization anisotropy in photoluminescence excitation and emission as well as Rayleigh scattering from individual and ensembles of polycrystalline CdTe nanowires aligned in polymer films. The results are in excellent agreement with finite-difference time domain calculations. We investigated a nanowire diameter regime in which a pronounced dependence of the polarization anisotropy on the diameter-wavelength ratio is observed which allows tuning of the optical anisotropies between its maximum predicted by the electrostatic limit to zero. We find that generally the polarization anisotropy in excitation is lower than in emission for materials with normal dispersion. Furthermore, the local refractive index of the environment changes the polarization anisotropy. Finally, the properties of individual nanowires can be fully transferred into macroscopically aligned polymer films. This opens opportunities for their large scale applications in polarization sensitive applications.

ACKNOWLEDGMENTS

Financial support by the DFG through the Nanosystems Initiative Munich (NIM), LMU*excellent*, and the SFB486 as well as by the China Scholarship Council (J.Z.) and the Alexander-von-Humboldt Foundation (A.A.L.) is gratefully acknowledged. We thank Alexander Govorov (Ohio University, USA) for fruitful discussions. A.L.R. also acknowledges the City University of Hong Kong (Project No. 7002551).

*Present address: Department of Physics and Materials Science, City University of Hong Kong, Tat Chee Avenue, Kowloon, Hong Kong.

†frank.jaeckel@physik.uni-muenchen.de

[1] Y. N. Xia, P. D. Yang, Y. G. Sun, Y. Y. Wu, B. Mayers, B. Gates, Y. D. Yin, F. Kim, and Y. Q. Yan, Adv. Mater. **15**, 353 (2003).

[2] Y. Li, F. Qian, J. Xiang, and C. M. Lieber, Mater. Today **9**, 18 (2006).

[3] T. Mélin and F. Laruelle, Phys. Rev. Lett. **81**, 4460 (1998).

[4] X. Duan and C. M. Lieber, Adv. Mater. **12**, 298 (2000).

[5] M. Kuno, Phys. Chem. Chem. Phys. **10**, 620 (2008).

[6] Z. Tang, N. A. Kotov, and M. Giersig, Science **297**, 237 (2002).

[7] J. F. Wang, M. S. Gudiksen, X. F. Duan, Y. Cui, and C. M. Lieber, Science **293**, 1455 (2001).

[8] C. Mauser, T. Limmer, E. Da Como, K. Becker, A. L. Rogach, J. Feldmann, and D. V. Talapin, Phys. Rev. B **77**, 153303 (2008).

[9] A. V. Maslov and C. Z. Ning, Phys. Rev. B **72**, 161310 (2005).

[10] F. Vouilloz, D. Y. Oberli, M.-A. Dupertuis, A. Gustafsson, F. Reinhardt, and E. Kapon, Phys. Rev. Lett. **78**, 1580 (1997).

[11] H. E. Ruda and A. Shik, J. Appl. Phys. **100**, 024314 (2006).

[12] H. Y. Chen, Y. C. Yang, H. W. Lin, S. C. Chang, and S. Gwo, Opt. Express **16**, 13465 (2008).

[13] J. Giblin, V. Protasenko, and M. Kuno, ACS Nano **3**, 1979 (2009).

[14] L. Cao, J. S. White, J.-S. Park, J. A. Schuller, B. M. Clemens, and M. L. Brongersma, Nature Mater. **8**, 643 (2009).

[15] T. Nobis, E. M. Kaidashev, A. Rahm, M. Lorenz, and M. Grundmann, Phys. Rev. Lett. **93**, 103903 (2004).

[16] L. Cao, B. Nabet, and J. E. Spanier, Phys. Rev. Lett. **96**, 157402 (2006).

[17] Y. P. Rakovich, Y. Volkov, S. Sapra, A. S. Susha, M. Döblinger, J. F. Donegan, and A. L. Rogach, J. Phys. Chem. C **111**, 18927 (2007).

[18] A. L. Rogach, T. Franzl, T. A. Klar, J. Feldmann, N. Gaponik, V. Lesnyak, A. Shavel, A. Eychmüller, Y. P. Rakovich, and J. F. Donegan, J. Phys. Chem. C **111**, 14628 (2007).

[19] B. M. I. van der Zande, L. Pages, R. A. M. Hikmet, and A. van Blaaderen, J. Phys. Chem. B **103**, 5761 (1999).

[20] A. Taflove and S. Hagness, *Computational Electrodynamics* (Artech House, Norwood, MA, 2000).

[21] A. F. Oskooi, D. Roundy, and M. Ibanescu, P. Bermel, J. D. Joannopoulos, and S. G. Johnson, Comput. Phys. Commun. **181**, 687 (2010).

[22] J. Zhang, A. A. Lutich, A. S. Susha, M. Döblinger, C. Mauser, A. O. Govorov, A. L. Rogach, F. Jäckel, and J. Feldmann, J. Appl. Phys. **107**, 123516 (2010).

[23] Polarization anisotropies were calculated from the fit parameters rather than from two individual polarizer orientations in order to obtain reliable results from the single NW experiments.

[24] L. Landau, E. Lifshitz, and L. Pitaevskii, *Electrodynamics of Continuous Media* (Elsevier Butterworth-Heinemann, Burlington, MA, 1984).

[25] *Handbook of Optical Constants of Solids II*, edited by E. D. Palik (Academic, Boston, USA, 1991).

[26] J. Garnett, Philos. Trans. R. Soc. London **203**, 385 (1904).

[27] J. C. Johnson, H. Yan, P. Yang, and R. J. Saykally, J. Phys. Chem. B **107**, 8816 (2003).

[28] H. Y. Li, S. Rühle, R. Khedoe, A. F. Koenderink, and D. Van-

maekelbergh, Nano Lett. **9**, 3515 (2009).
[29] F. Balzer, V. G. Bordo, A. C. Simonsen, and H.-G. Rubahn, Phys. Rev. B **67**, 115408 (2003).
[30] J. Lee, P. Hernandez, J. Lee, A. O. Govorov, and N. A. Kotov, Nature Mater. **6**, 291 (2007).
[31] J. Hu, L.-s. Li, W. Yang, L. Manna, L.-w. Wang, and A. P. Alivisatos, Science **292**, 2060 (2001).
[32] M. van Gurp, G. van Ginkel, and Y. K. Levine, J. Polym. Sci., Part B: Polym. Phys. **26**, 1613 (1988).